Hindawi
Journal of Nanomaterials
Volume 2022, Article ID 8929985, 10 pages
https://doi.org/10.1155/2022/8929985

Research Article

Entropy Generation Analysis for MHD Flow of Hybrid Nanofluids over a Curved Stretching Surface with Shape Effects

Basharat Ullah,[1] **Umar Khan**,[1] **Hafiz Abdul Wahab**,[1] **Ilyas Khan**,[2] **and Md. Nur Alam**[3]

[1]*Department of Mathematics and Statistics, Hazara University, Mansehra 21120, Pakistan*
[2]*Department of Mathematics, College of Science, Al-Zulfi, Majmaah University, Al-Majmaah 11952, Saudi Arabia*
[3]*Department of Mathematics, Pabna University of Science & Technology, Pabna 6600, Bangladesh*

Correspondence should be addressed to Hafiz Abdul Wahab; wahab@hu.edu.pk and Md. Nur Alam; nuralam.pstu23@gmail.com

Received 9 September 2021; Accepted 30 May 2022; Published 15 June 2022

Academic Editor: Iaroslav Gnilitskyi

The characteristic of magnetohydrodynamic flow of viscous fluids is explained here. The energy equation behavior is studied in the presence of heat, viscous dissipation, and joule heating. The major emphasis of this study is the physical behavior of the entropy optimization rate. Based on the implementation of curvilinear coordinates, the basic flow equations are established. Nonlinear partial differential expressions are reduced by appropriate transformation to the ordinary differential system. In the engineering and industrial processes, nanoparticles and their shape have practical consequences. For this reason, we give a detailed investigation of the shape impacts on the flow through the curved stretching surface of nanoparticles. The flow equations are reduced into a number of nonlinear differential equations which are solved numerically using a useful numerical approach called Runge-Kutta-4 (RK-4). The shooting method is first used to reduce the equations to a number of problems of first order, and then the RK-4 approach is used for solution. Impacts for entropy optimization, Bejan number, velocity, concentration, and temperature of several physical parameters are graphically studied.

1. Introduction

During the last few decades, extensive surfaces have been received by researchers. This is due to its extensive uses in mining, metallurgy, and engineering. In the production processes, sheet stretching has certain activities with respect to product characteristics. These applications are important in different real-life processes due to different stretching speeds such as rubber-plating flow generation, metal casting continuous, fiber spinning, paper products, glass blowing and fiber, wire drawing, and polymer sheeting. Due to viscous dissipation, the distribution of the temperature changes as a source of energy, which results in changes in the heat conductivity. Several researchers have recently been interested in developing and designing new cooling/heating equipment and machines.

In magnetohydrodynamic fluid flow, Rashidi et al. [1] highlight the impacts of thermal fluxes and the mixtures by means of a porous stretching sheet. Swain et al. [2] have investigated the heating transmission behaviors in a porous medium for MHD flow in an exponentially expanding sheet. Thermal flux effects and Eid et al. [3] present magnetohydrodynamics in Carreau nanomaterials, which float a porous, nonlinear stretch sheet. Sheikholeslami et al. [4] analyzed the stretchable and forced surface flow of nanomaterials from MHD. The main results of the study demonstrate that radiation parameter improvement reduces the heat transfer rate. Imtiaz et al. [5] examine the effect of the chemical reaction to quartic autocatalysis in magnetohydrodynamic flow from a curved stretchable surface. Hayat et al. [6] analyzed viscous fluid MHD flow over a nonlinear curved, heat generation/absorption stretchable surface.

Usman et al. [7] demonstrate electromagnetic couple stress film flow of hybrid nanofluid over an unsteady rotating disc. Hayat et al. [8] examine the effect of thermal rays and chemical reactions on MHD convective flow through a curved stretching surface. Abbas et al. [9] investigate the flow of hydrodynamic nanomaterial by means of a curved thermal stretching field. The first step was taken to propose

an analytical model for the therapeutic efficiency of nanofluids. This model contains the concentration of nanoparticles and the thermal conductivity of the base fluid and nanoparticles.

Moreover, only spherical nanoparticle inclusions are required. Hamilton suggested a model for nonsphere-shaped nanoparticles to address this deficiency. Further studies are carried out in this area with a variety of models exploring nanoparticles sort [10–12], particulate form [13], particle size [14], and others. Furthermore, many scientists would also be interested in various heat transfer mechanisms, including Brownian particle motion [15], accumulation of particles [16, 17], and liquid layers [18].

While nanofluids can live up to the thermal efficiency thirst, researchers are still searching for different fluid forms. Hybrid nanofluids are hybrid nanofluid types with excellent thermal performance compared with nanofluids. These fluids were created by scattering into a base fluid two or more types of little particles inside the base fluid or composite nanostructures. This means that the homogeneous mixture of different products hardly could be imagined in a single substance, with the physicochemical properties [19]. The active role of hybrid nanofluids in the various applications of heat transfer is as follows: electronic cooling, automotive radiators, cooling generators, nuclear coolers, machining coolants, lubrications, solar heat, thermal storage, building heating, biomedical treatments, drug control, cooling, and protection. There are positive industrial characteristics, such as chemical stability and high thermal efficiency, which permit the efficient performance of nanofluids.

The measurement of entropy is used to explain the efficiency of many engineering and industrial systems. Various scientists and engineers therefore based their attention on the question of entropy. The sum of any sort of energy produced by a system or its surrounding irreversible processes is called entropy production. It is not necessary to use this energy for a successful operation. The second law of thermodynamics is used for entropy production. In contrast to the first law, Thermodynamics' second legislation is more effective. Irreversible processes include liquid flux due to resistance flux, diffusion, game heating, viscous fluid rubbing, chemical reaction, thermal radiation, etc. We regulated the entropy generation rate to boost the system's performance. The second law of thermodynamics states that entropy values must be null or larger within a system than 0. The enteropy rate considering the porosity effect was discussed by Ajibade et al. [20]. The effects of entropy production caused by heat transmission over flat surfaces or stretching plates have examined by numerous researchers [21, 22], but few studies have found in the literature related to the investigation about rate of entropy production with thermal effects in the flow past stretching cylinders. Our current article theoretically examines transmission of thermal energy over a stretching cylinder using heat generation/absorption and Joule heating. Moreover, this work also investigates rate of entropy generation for the spinning flow system.

Entropy production eliminates the usable energy in the system in many engineering and industrial processes. In order to maximize energy in the system for efficient system operation, it is therefore imperative to evaluate the rate of entropy generation in a system. Under the second thermodynamics theorem, all processes of flow and heat transfer undergo irreversible changes. The main cause of these irreversible changes is the lack of control during the processes. While steps to minimize these irreversible effects can be taken, all the energy lost cannot be recovered. The entropy of the system is increased by this process. This results in a standard metric for the investigation of the irreversibility effects of entropy generation rate. Bejan suggested this approach [23, 24]. Khan et al. [25] recently studied the entropy analysis in a curved tube.

This research is intended by means of a curved stretching surface to address entropy generation in MHD vincent fluid flow. Fluid velocity and temperature similarity solutions are obtained, and the reduced equation structure is numerically resolved by a Runge-Kutta shooting algorithm method. The effects of the various interesting variables are studied on the optimization of entropy, speed, number of Bejan, and temperature. The findings were subsequently described in graphical form along with a quantitative discussion about the embedded parameters.

2. Description of the Problem

Take a two-dimensional flow into a curved stretching sheet from an incompressible magnetohydrodynamic (MHD) viscous fluid. In a circle with radius R, the extension sheet is curved. The s-direction is perpendicular to the fluid motion direction along the stretching surface with the stretching velocity $U_w(s) = as\,(a > 0)$ and r-direction. In the r direction, the magnetic field (B_0) is applied. The flow chart is shown in the Figure 1.

$$\frac{\partial}{\partial r}(r+R) + v + R\frac{\partial u}{\partial x} = 0, \tag{1}$$

$$\frac{u^2}{r+R} = \frac{1}{\rho_{\text{hnf}}}\frac{\partial H}{\partial r}, \tag{2}$$

$$\begin{aligned} v\frac{\partial u}{\partial r} + \frac{uR}{r+R}\frac{\partial u}{\partial s} + \frac{uv}{r+R} &= -\frac{1}{\rho_{\text{hnf}}}\frac{R}{r+R}\frac{\partial H}{\partial s} + \nu_{hnf}\left(\frac{\partial^2 u}{\partial r^2} + \frac{1}{r+R}\frac{\partial u}{\partial r} - \frac{u}{r+R^2}\right) \\ &\quad - \frac{\sigma {B_0}^2}{\rho_{\text{hnf}}}u, \end{aligned} \tag{3}$$

$$\begin{aligned} v\frac{\partial T}{\partial r} + u\frac{\partial T}{\partial s}\frac{R}{r+R} &= \frac{\alpha_{\text{hnf}}}{(\rho c_p)_{\text{hnf}}}\left(\frac{\partial^2 T}{\partial r^2} + \frac{1}{r+R}\frac{\partial T}{\partial r}\right) \\ &\quad + \frac{\sigma {B_0}^2}{(\rho c_p)_{\text{hnf}}}u^2 + \frac{\mu_{\text{hnf}}}{(\rho c_p)_{\text{hnf}}} \\ &\quad \cdot \left(\left(\frac{\partial u}{\partial r}\right)^2 + \left(\frac{u}{r+R}\right)^2\right) \\ &\quad + \frac{Q_0}{(\rho c_p)_{\text{hnf}}}(T - T_\infty). \end{aligned} \tag{4}$$

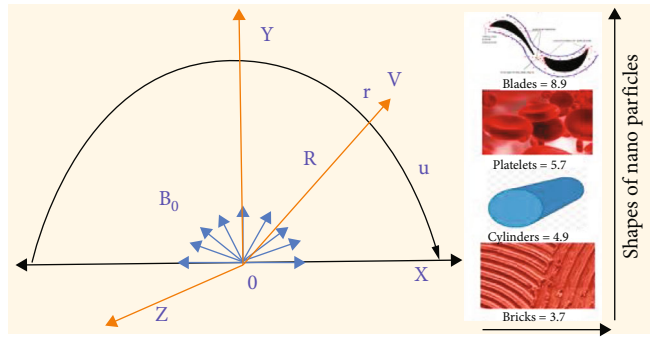

Figure 1: Geometry of problem.

Table 1: Thermophysical properties of nanofluid and hybrid nanofluid (see ref. [28]).

Properties	Nanofluid	Hybrid nanofluid
Density	$\rho_{nf} = (1-\phi) + \phi_2\rho_s$	$\rho_{\text{hnf}} = (1-\phi_2)\left[\left((1-\phi_2)\rho_f + \phi_1\rho_{s1}\right)\right] + \phi_2\rho_{s2}$
Heat capacity	$(\rho C_p)_{nf} = (1-\phi)(\rho C_p)_f + \phi(\rho C_p)_s$	$\left(\rho_{cp}\right)_{\text{hnf}} = (1-\phi_2)\left[(1-\phi_1)\left(\rho_{cp}\right)_f + \phi_1\left(\rho_{cp}\right)_{s_1}\right] + \phi_2\left(\rho_{cp}\right)_{s_2}$
Viscosity	$\mu_{nf} = \dfrac{\mu_f}{(1-\varnothing)^{2.5}}$	$\mu_{\text{hnf}} = \dfrac{\mu_f}{(1-\phi_1)^{2.5}(1-\phi_2)^{2.5}}$
Thermal conductivity	$\dfrac{k_{nf}}{k_f} = \dfrac{k_s + (n-1)k_f - (n-1)\phi(k_f - k_s)}{k_s + (n-1)k_f + \phi(k_f - k_s)}$	$\dfrac{k_{\text{hnf}}}{k_{bf}} = \dfrac{k_{s_2} + (n-1)k_{bf} - (n-1)\phi_2(k_{bf} - k_{s_2})}{k_{s_2} + (n-1)k_{bf} + \phi_2(k_{bf} - k_{s_2})}$ where $k_{bf}/k_f = k_{s_1} + (n-1)k_f - (n-1)\phi_1(k_f - k_{s_1})/k_{s_1} + (n-1)k_f + \phi_1(k_f - k_{s_1})$

$$u = U_w = as, v = 0, T = T_w = T_\infty \text{ at } r = 0, \tag{5}$$

$$u \longrightarrow 0, \frac{\partial u}{\partial r} \longrightarrow 0, T = T_\infty \, at \, r \longrightarrow \infty, \tag{6}$$

in which Eq. (1) reflects the preservation in the presence of transverse magnetic fields of mass, transverse, and axial components to preserve linear momentum in Eqs. (2) and (3), respectively. Furthermore, the energy equation defined in Eq. (4) will be used to analyze heat transfer. In addition, u and v denote s-and r-direction velocity components, H pressure, ρ_{hnf} hybrid nanofluid density, ν kinematics viscosity, μ dynamic viscosity, B_0 strength of the magnetic field, σ electric conductivity, T and T_∞ surface temperatures and environmental temperatures, and Q_0 heat generation, respectively. The transformation is used [26, 27]. Moreover, thermophysical properties of nanofluid and hybrid nanofluid, thermophysical properties of water, ethylene, and copper are displayed in Tables 1 and 2, respectively, which illustrate the effective property of Al_2O_3 /water-based nanofluid and Cu/Al_2O_3 hybrid nanofluid.

$$u = as f'(\zeta), v = -\frac{R}{r+R}\sqrt{av} f(\zeta), \theta(\zeta) = \frac{T - T_\infty}{T_w - T_\infty},$$
$$H = \rho a^2 s^2 H(\zeta), \zeta = \sqrt{\frac{a}{v}} r. \tag{7}$$

The general relationship used to compute the density and specific heat for nanofluids (Brikman's model). The dynamic effective viscosity and the effective thermal conductivity are used by several researchers for many nanofluids and Maxwell's effective thermal conductivity model for two-phase mixtures.

Now, Eq. (1) is automatically verified, and Eqs. (2)–(4) are transformed to nondimensional ordinary differential equations as follows.

$$\left(\frac{1}{\psi_1}\right) H'(\zeta) = \frac{1}{\zeta + B} f' 2, \tag{8}$$

$$\left(\frac{1}{\psi_1}\right)\frac{2B}{\zeta + B} H = \left(\frac{1}{\psi_2}\right)\left(f''' + \frac{1}{\zeta + B} f'' - \frac{B}{(\zeta + B)^2} f' - \frac{B}{\zeta + B} f'^2\right) + \frac{B}{\zeta + B} f f'' + f f' \frac{B}{(\zeta + B)^2} - M f', \tag{9}$$

$$\frac{1}{\psi_3}\left(\theta'' + \frac{1}{\zeta + B}\theta'\right) + \frac{k_{hnf}}{k_{bf}}\left(MBr\left(f'^2 + \left(\frac{1}{\psi_4}\right)\left(f''^2 + \frac{1}{(\zeta + B)^2} f'^2\right)\right) + \Pr\frac{B}{\zeta + B} f\theta'\right) = 0, \tag{10}$$

Table 2: Thermophysical properties of water, ethylene, and copper (see ref. [29]).

Properties	Water	Al_2O_3	Cu
$\rho\left(\frac{kg}{m^3}\right)$	997.0	3970	8933
$C_p\left(\frac{J}{kgK}\right)$	4180	765	385
$k\left(\frac{W}{mK}\right)$	0.6071	40	400

in which

$$\psi_1 = \frac{\rho_{hnf}}{\rho_f} = (1-\phi_2)\left[\left((1-\phi_1)+\phi_1\frac{\rho_{s1}}{\rho_f}\right)\right]+\phi_2\frac{\rho_{s2}}{\rho_f}, \quad (11)$$

$$\psi_2 = \frac{\nu_f}{\nu_{hnf}} = (1-\phi_1)^{2.5}(1-\phi_2)^{2.5}\left\{\left((1-\phi_2)(1-\phi_1)+\phi_1\frac{\rho_{s1}}{\rho_f}\right)\right\}+\phi_2\frac{\rho_{s2}}{\rho_f}, \quad (12)$$

$$\psi_3 = \frac{\left(\rho_{cp}\right)_{hnf}}{\left(\rho_{cp}\right)_f} = (1-\phi_2)\left[(1-\phi_1)+\phi_1\frac{\left(\rho_{cp}\right)_{s_1}}{\left(\rho_{cp}\right)_f}\right]+\phi_2\frac{\left(\rho_{cp}\right)_{s_2}}{\left(\rho_{cp}\right)_f}, \quad (13)$$

$$\psi_4 = \frac{\mu_{hnf}}{\left(\rho_{cp}\right)_{hnf}} = (1-\phi_1)^{2.5}(1-\phi_2)^{2.5}\left[(1-\phi_1)+\phi_1\frac{\left(\rho_{cp}\right)_{s_1}}{\left(\rho_{cp}\right)_f}\right]+\phi_2\frac{\left(\rho_{cp}\right)_{s_2}}{\left(\rho_{cp}\right)_f}. \quad (14)$$

Eliminating pressure H from Eqs. (8) and (9), we get

$$f^{iv}+\frac{2}{\zeta+B}f'''-\frac{1}{(\zeta+B)^2}f''+\frac{1}{(\zeta+B)^3}f'-(\psi_2)\left(\frac{B}{(\zeta+B)}ff''+\frac{B}{(\zeta+B)}ff'''\right)-\frac{B}{(\zeta+B)^2}f'2+\frac{B}{(\zeta+B)^2}ff''-\frac{B}{(\zeta+B)^3}ff'-\frac{M}{\psi_1}\left(\frac{1}{(\zeta+B)}f'+f''\right)=0. \quad (15)$$

The transformed boundary conditions are as follows:

$$f=0, f'=1, \theta=1\ at\ \zeta=0\ f'\longrightarrow 0, f''\longrightarrow 0, \theta\longrightarrow 0\ as\ \zeta\longrightarrow\infty. \quad (16)$$

In the above relations, $\Pr=\nu_{hnf}/\alpha_{hnf}$ depicts the Prandtl number, $M=(\sigma B_0{}^2/a\rho_{hnf})$ the Hartmann number, $Ec=(a^2s^2/(c_p)_{hnf}(T_w-T_\infty))$ the Eckert number, $Br=(\mathrm{PrEc})$ the Brinkman number, and $\beta=(Q_0/a(\rho c_p)_{hnf})$ the heat generation/absorption parameter, and $B=\sqrt{a/\nu}$, R, is the curvature parameter.

2.1. Skin Friction Coefficient and Local Nusselt Number. The physical quantities of interest are skin friction coefficient C_f and local Nusselt number Nu_s, which are define as follows:

$$C_f=\frac{\tau_{rs}}{\rho_{hnf}u^2{}_w}, Nu_s=\frac{sq_w}{k_{hnf}(T_w-T_\infty)}, \quad (17)$$

where the wall fraction τ_{rs} and heat transfer q_w along the s-direction are define as follows:

$$\tau_{rs}=\mu_{hnf}\left(\frac{\partial u}{\partial r}-\frac{u}{r+R}\right)\Big|_{r=0}, q_w=-k_{hnf}\left(\frac{\partial T}{\partial r}\right)\Big|_{r=0}. \quad (18)$$

In view of Eq. (7), expressions describe in Eq. (17) provide dimensionless skin friction and Nusselt as follows:

$$\left(\frac{Re_s}{2}\right)^{1/2}C_f=\frac{1}{(1-\phi_2)}\left(f''(0)-\frac{1}{B}f'(0)\right), \quad (19)$$

$$\frac{L}{s}\left(\frac{Re_s}{2}\right)^{-1/2}Nu_s=-\frac{k_{hnf}{}'}{k_f}[\theta(0)], \quad (20)$$

where $Re_s=\sqrt{a/\nu}s$ elucidates local Reynolds number.

2.2. Entropy Generation Equation. Measuring any sort of energy created in irreversible systems processes is referred to as the generation of entropy. Entropy generation is described in dimensional form:

$$S_G=\frac{k_{hnf}}{T_\infty{}^2}\left(\frac{\partial T}{\partial r}\right)^2+\frac{\mu_{hnf}}{T_\infty}\left(\frac{\partial u}{\partial r}+\frac{u}{r+R}\right)^2+\frac{\sigma B_0{}^2}{T_\infty}u^2. \quad (21)$$

Dimensionless version satisfies

$$N_G=\alpha_1\theta'^2+\mathrm{MB}rf'^2+Br\left(f'{}'^2+\frac{1}{(\zeta+B)^2}f'^2+\frac{1}{\zeta+B}f'f''\right). \quad (22)$$

Bejan number is expressed as follows:

$$\mathrm{Be}=\frac{\text{Heat and mass transfer irreversibility}}{\text{Total Irreversibility}} \quad (23)$$

or

$$Be = \frac{\alpha_1 \theta'^2}{\alpha_1 \theta'^2 + \mathrm{MB}rf'^2 + Br\left(f'''^2 + \left(1/(\zeta + B)^2\right)f'^2 + (1/\zeta + B)f'f''\right)}. \tag{24}$$

Here, $N_G = (S_G T_\infty \nu / ak(T_w - T_\infty))$ denotes the entropy generation rate, $\alpha_1 = (T_w - T_\infty / T_\infty)$ the temperature difference parameter, and $Br = \mu_{hnf}(as)^2/k(T_w - T_\infty)$ the Brinkman number.

For the sake of comparison, we have also solved the same problem by using the R-K-4 method (coupled with shooting technique), and the results are compared in Table 3. Both solutions show an excellent agreement with each other. These solutions are calculated for $\beta = M = Br = 0.1$ and $\phi 1 = \phi 2 = 0$, and Prandtl number is taken to be 6.2.

3. Physical Description

In this section, we investigate the comportations of several interesting parameters for entropy optimization, velocity, number of Bejan, skin friction, and heat transfer rates.

3.1. Velocity Profile. For the velocity of different values, Figures 2–4 are shown. Changes of the axial velocity variable of dimensionless dimensions are shown in Figure 2, for B. The fluid velocity is also increased as the curvature parameter (B) is increased. This means that when compared to the straight layer, the velocity of the curved layer is insufficient. This shift in velocity is much higher in shape.

The effect of M on velocity is plotted in Figure 3. Figure 3 shows that the parameter of M plays a role in this point. The explanation is that the fluid movement is due to the surface extension, and that any fluid change on the stretching surface helps decelerate the fluid flow. Moreover, it is apparent from this figure that for different form variables, the decrease in velocity occurs slightly greater.

Figure 4 is plotted to evaluate the effect on the velocity of varying shape variables of volumetric fractions ϕ_2. From this figure, it is assumed that for shape variables, the velocity profile decreases in dominant.

3.2. Temperature Profile. The influences of B, β, Br, M and ϕ_2 on $\theta(\zeta)$ are plotted in Figures 5–9. The influence of these parameters on $\theta(\zeta)$ is under discussion in the curved stretching surface. In addition, there are four distinct shape factors plotted for each graph. Figure 5 shows that (B) has a decreasing $\theta(\zeta)$ role to play. This is because the fluid acceleration is caused by surface stretching, and so any fluid (B) change on the stretching surface causes the fluid to decelerate. Furthermore, it is evident from this figure that the decrease in range $\theta(\zeta)$ is slightly more for different shape factors results.

Figure 6 is plotted to check the parameter (β) for temperature effect. Through this calculation, it is discovered that the temperature increases with (β). It is because the improvement in (β) value strengthens the conduction effects and thereby increases the temperature. In the field outside the surface, the rise is prevalent and leads to the rising heat flux in the soil. Hybrid nanofluid-shape blade nanoparticles have the highest temperature and the lowest temperature of nanofluid nanoparticles formed by bricks. Furthermore, these effects are more massive than nanofluid in the case of hybrid nanofluids because hybrid nanofluid is more thermal than nanofluids.

Figure 7 indicates the effect of the parameter for the Brinkman number Br. From this figure, the parameter of heat generation is presumed to slowly affect the distribution of temperature. It is because it implies that the surface

Table 3: Comparison between present result and ref. [25]].

M	B	Ref [25]]	Current result
0.2	0.8	6.975	6.9751
0.3		5.968	5.9683
0.4		5.123	5.1232
0.5	0.0	4.937	4.9371
	0.5	5.128	5.1283
	1.0	5.342	5.3422

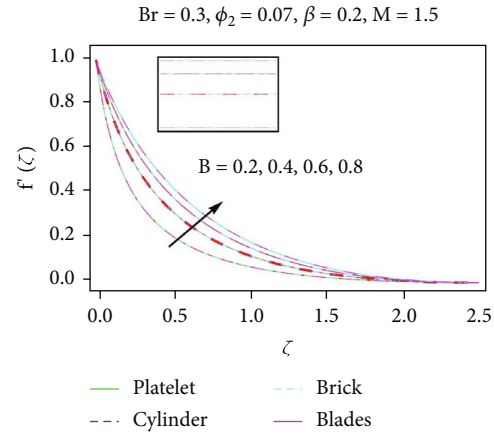

Figure 2: Impact of B on velocity.

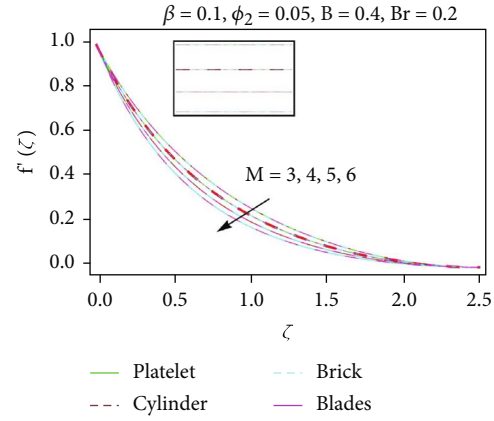

Figure 3: Impact of M on velocity.

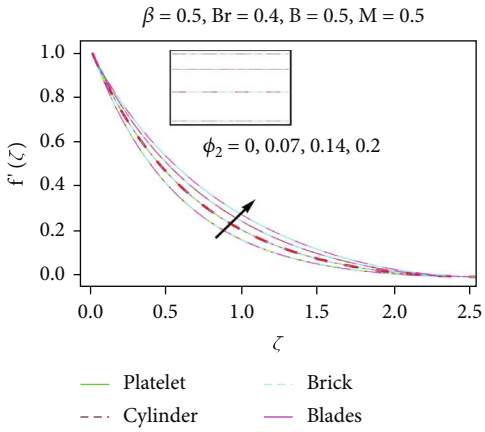

Figure 4: Impact of ϕ_2 on velocity.

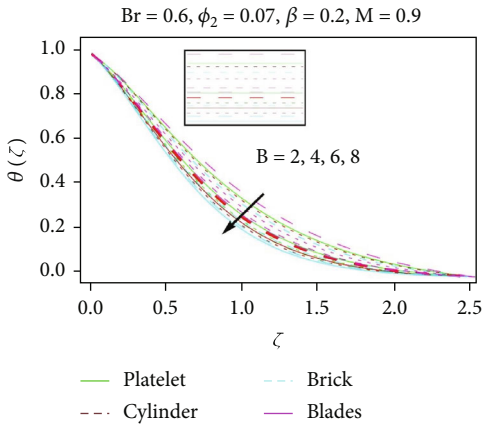

Figure 5: Impact of B on temperature.

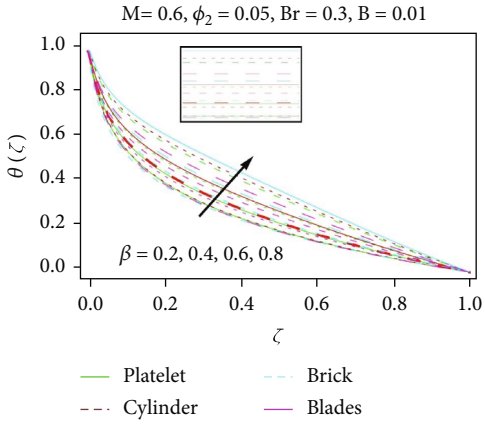

Figure 6: Impact of β on temperature.

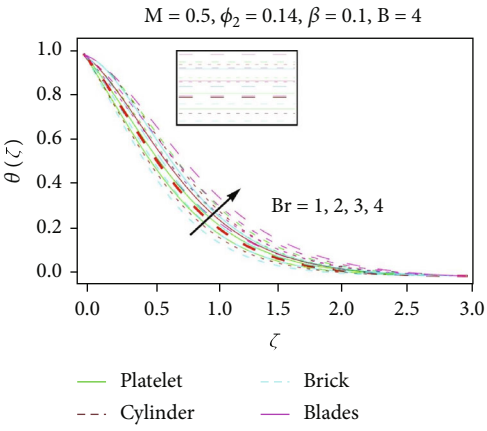

Figure 7: Impact of Br on temperature.

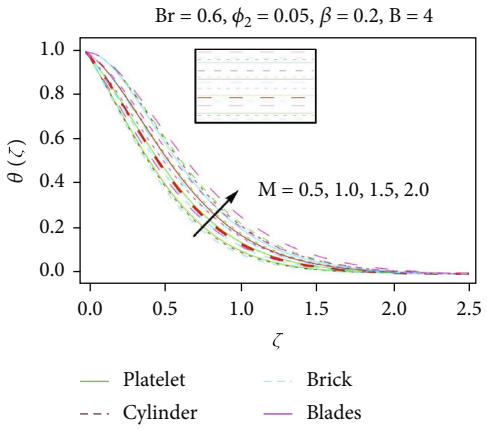

Figure 8: Impact of M on temperature.

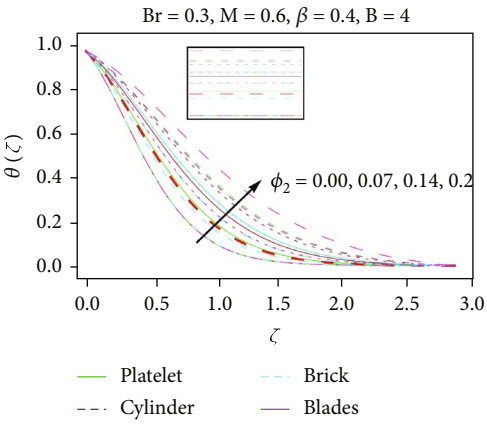

Figure 9: Impact of ϕ_2 on temperature.

temperature is above the ambient temperature, and more heat is transferred to the fluid from the ambient, which contributes to thermal boundary layer thickness and increasing temperature. In the case of hybrid nanofluid, this temperature rise is also assumed to predominate. The maximum temperature for blade-shaped nanofluid nanoparticles is achieved; for brick-shaped nanofluid nanoparticles, the lowest temperature magnitude is noted.

The variance of the Hartmann number (M) on $\theta(\zeta)$ is shown in Figure 8. Here, we have found that higher (M) values lead to an increase in $\theta(\zeta)$ thickness and thermal boundaries. The implication is that the resistive force (force

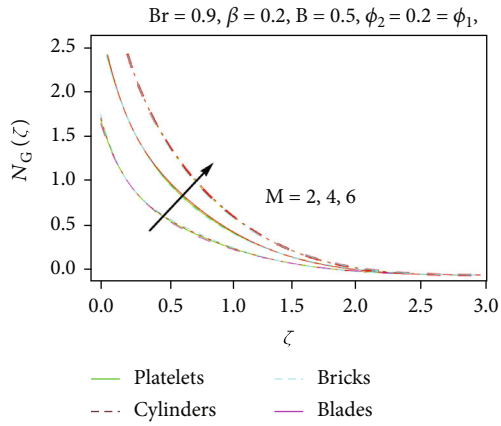

Figure 10: Impact of M on entropy generation.

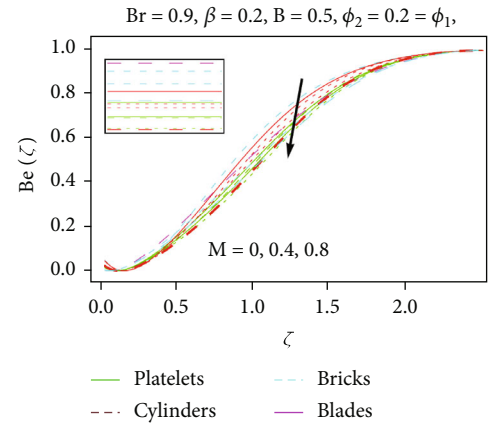

Figure 11: Impact of M on Bejan number.

Lorentz) increases with a higher value of M and therefore increases the temperature.

Figure 9 demonstrates the influence of volumetric fractions ϕ_2 on temperature. It is expected that the thickness of both the temperature and thermal boundary layer would grow with an increase of ϕ_2. That is because ϕ_2 contributes to the deceleration of fluid flow and contributes indirectly to the magnitude of rising temperature. The temperature magnitude for hybrid nanofluids is also evident from this figure to be higher for the values of ϕ_2 than for the nanofluid value. In addition, hybrid nanofluid blade-shaped nanoparticles have a high temperature, and brick-shaped nanofluid nanoparticles have the lowest temperature.

3.3. Entropy Generation. Impacts on N_G and Be are examined in this section of a Hartmann number (M), Brinkman number (Br), and ϕ_2 volumetric fractions. Figures 10 and 11 illustrate the impact of Hartmann number (M) on N_G and Be. Increased entropy generation (N_G) in M is reported. Because of the fact that for higher (M), the force of Lorentz creates greater resistance to fluid movement, and the entropy (N_G) increases as expected. The Bejan number (Be) was reduced compared to larger numbers (M) of Hartmann.

The behavior of Brinkman number (Br) on N_G and Be is illustrated in Figures 12 and 13. More (Br) values are more entropy-generated (N_G). In fact, the thermal conductivity decreases for higher estimates (Br), and thus an increase is shown with the entropy optimization process. The counter effect is for (Br) the Bejan number (Be). The number of Bejan is the largest value if the number of Brinkman is zero and decreases accordingly (Br).

Figures 14 and 15 are sketched for the impact of volumetric fractions ϕ_2 against (N_G) and (Be). It is noticed that the entropy of fluid increases for larger (N_G) while Bejan number (Be) reduces.

3.4. Engineering Quantities. In the final part of this section, Figures 16–19 are plotted to test the effect of different shape factor values in terms of variations of different embedded parameters on the local Nusselt number and skin friction. Numerous values of ϕ_2 were decorated with the horizontal

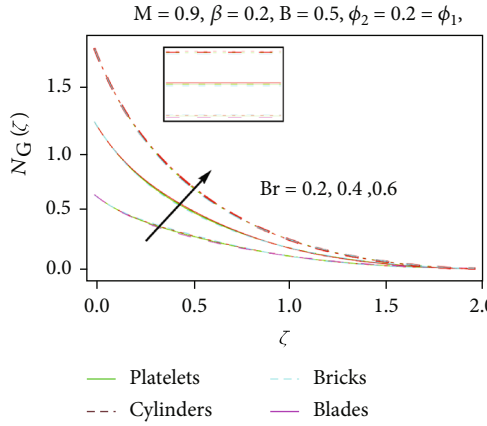

Figure 12: Impact of Br on entropy generation.

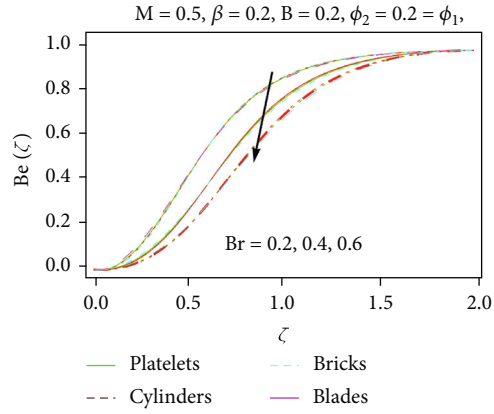

Figure 13: Impact of Br on Bejan number.

axis. From Figure 16, the case where the injection is paired with contraction, the parameter β increases the skin friction, while the parameter ϕ_2 shows a reversed behavior.

In addition, nanostructures formed by the blades possess high heat transmission. Figure 17 is plotted for the different values of M, which indicate the same corresponding analysis

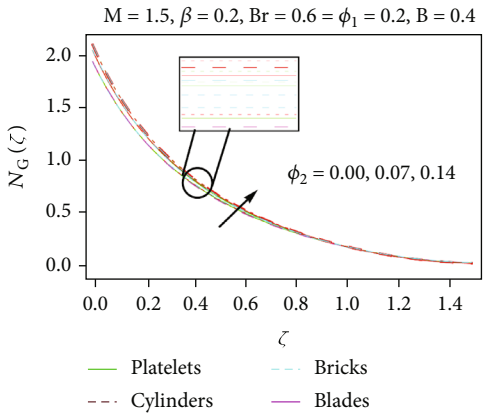

Figure 14: Impact of ϕ_2 on entropy generation.

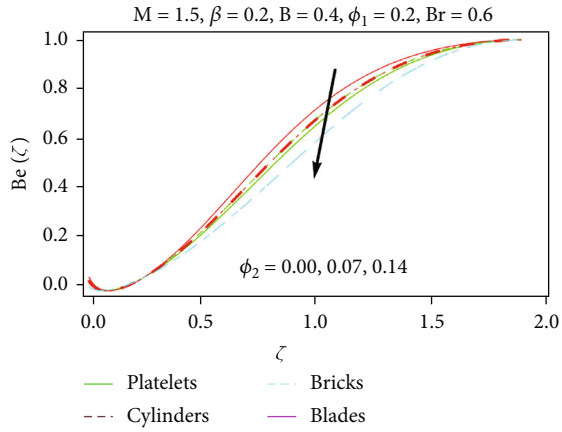

Figure 15: Impact of ϕ_2 on Bejan number.

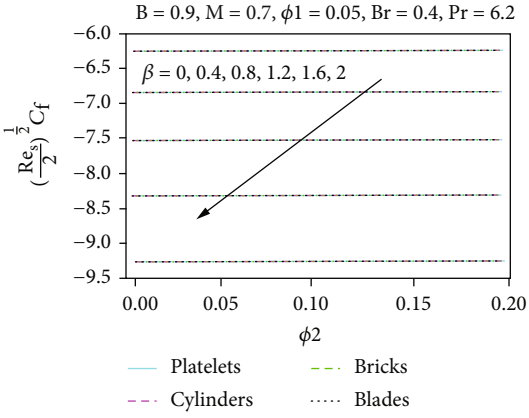

Figure 16: The variation of skin friction for varying $\phi 2$ and β.

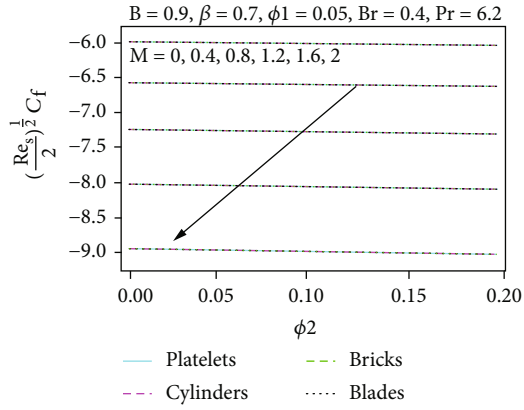

Figure 17: The variation of skin friction for varying $\phi 2$ and M.

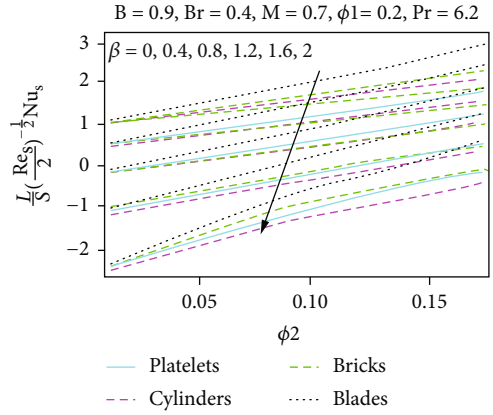

Figure 18: The variation of Nusselt number for varying $\phi 2$ and β.

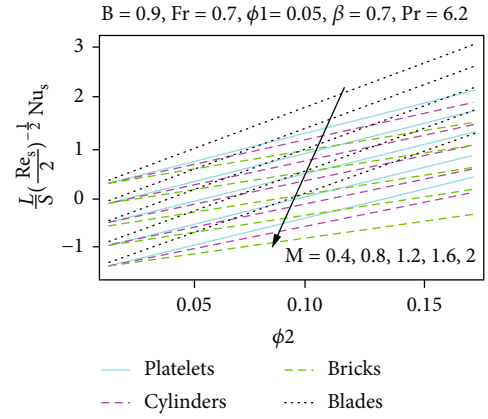

Figure 19: The variation of Nusselt number for varying $\phi 2$ and M.

in Figure 16. Again, it has been found that nanocomposite-shaped blades are more capable of transferring heat than tiny particles formed by platelets, cylinders, or bricks.

Figures 18 and 19 show the effect ϕ_2, M, and β on the local heat transfer rate. Figure 18 shows that the local heat transfer rates decrease, as the value of ϕ_2 increases. For blade-shaped nanoparticles, the rates are higher and against β are indicated.

The changes in the local number of Nusselt due to the increasing number of Hartmann (M) are seen in Figure 19. It is found that nanoparticles formed by brick which decreases in the local heat transfer rate are lower than the others.

4. Conclusions

In this paper, the object of the present study is to analyze entropy generation with a curved stretcher surface of MHD flow of viscous fluids for several small particles. The findings of this study are concluded.

(1) The velocity in the case of blade and brick small particles is noted to be rapidly increased

(2) The fluid temperature increases quite slowly for platelet-shaped particles, and the rest of the nanoparticles show quit rapidly increases behavior

(3) Enhancement in the curvature parameter increases the velocity profile, whereas the temperature profile diminishes

(4) The heat generation parameter and Hartmann number contribute in lowering the magnitude of Nusselt number and increase in thermal radiation parameter and increase the magnitude of Nusselt number for both nano and hybrid nanofluids, respectively. Moreover, the magnitude of Nusselt number is slightly more in case of nanofluid as compare to hybrid nanofluid

(5) Temperature and velocity profiles showed increasing activity in order to estimate the solid volume fraction

(6) One of the essential sources of entropy production is a curved stretching sheet

(7) For (Br) and (M), NG shows the same results

(8) For higher (M) and (Br) numbers, (Be) is reduced

Nomenclature

u: Component of velocity in the x direction
v: Component of velocity in the y direction
ρ_{hnf}: Density of hybrid nanofluid
B_0: Strength of the magnetic Field
H: Pressure
μ: Dynamic viscosity
ν: Kinematics viscosity
σ: Electric conductivity
T: Surface temperatures
T_∞: Environmental temperatures
Q_0: Heat generation
ρ_{nf}: Density of nanofluid
ρs: Density of solid particle
ϕ_1, ϕ_2: Volume fraction of nanoparticles and hybrid nanoparticles
kf: Conductivity of the base fluid
θ: Dimensionless temperature
m: Shape factor of nanoparticles
ζ: Dimensionless variable
Cf: Skin friction coefficient
Nu: Nusselt number
Br: Brinkman number
Ec: Eckert number
B: Curvature parameter
Pr: Prandtl number
M: Hartmann number
N_G: Entropy generation rate
α_1: The temperature difference parameter
Be: Bejan number.

Data Availability

The study based on numerical technique and no data is used in findings of the study.

Conflicts of Interest

The authors declare that they have no conflicts of interest.

References

[1] M. M. Rashidi, B. Rostami, N. Freidoonimehr, and S. Abbasbandy, "Free convective heat and mass transfer for MHD fluid flow over a permeable vertical stretching sheet in the presence of the radiation and buoyancy effects," *Ain Shams Engineering Journal*, vol. 5, no. 3, pp. 901–912, 2014.

[2] I. Swain, S. Mishra, and H. Pattanayak, "Flow over Exponentially Stretching Sheet through Porous Medium with Heat Source/Sink," *Journal of Engineering*, vol. 2015, 7 pages, 2015.

[3] M. Eid, K. Mahny, T. Muhammad, and M. Sheikholeslami, "Numerical treatment for Carreau nanofluid flow over a porous nonlinear stretching surface," *Results in physics*, vol. 8, pp. 1185–1193, 2018.

[4] M. Sheikholeslami, M. Mustafa, and D. Domiri Ganji, "Effect of Lorentz forces on forced-convection nanofluid flow over a stretched surface," *Particuology*, vol. 26, pp. 108–113, 2015.

[5] M. Imtiaz, T. Hayat, A. Alsaedi, and A. Hobiny, "Homogeneous-heterogeneous reactions in MHD flow due to an unsteady curved stretching surface," *Journal of Molecular Liquids*, vol. 221, pp. 245–253, 2016.

[6] T. Hayat, R. Saif, R. Ellahi, T. Muhammad, and B. Ahmad, "Numerical study of boundary-layer flow due to a nonlinear curved stretching sheet with convective heat and mass conditions," *Results in physics*, vol. 7, pp. 2601–2606, 2017.

[7] M. Usman, T. Gul, A. Khan, A. Alsubie, and M. Z. Ullah, "Electromagnetic couple stress film flow of hybrid nanofluid over an unsteady rotating disc," *International Communications in Heat and Mass Transfer*, vol. 127, article 105562, 2021.

[8] T. Hayat, M. Rashid, M. Imtiaz, and A. Alsaedi, "MHD convective flow due to a curved surface with thermal radiation and chemical reaction," *Journal of Molecular Liquids*, vol. 225, pp. 482–489, 2017.

[9] Z. Abbas, M. Naveed, and M. Sajid, "Hydromagnetic slip flow of nanofluid over a curved stretching surface with heat generation and thermal radiation," *Journal of Molecular Liquids*, vol. 215, pp. 756–762, 2016.

[10] N. S. Khan, P. Kumam, and P. Thounthong, "Magnetic field promoted irreversible process of water based nanocomposites with heat and mass transfer flow," *Scientific Reports*, vol. 11, no. 1, pp. 1–25, 2021.

[11] N. S. Khan, L. Ali, R. Ali, P. Kumam, and P. Thounthong, "A novel algorithm for the computation of systems containing different types of integral and integro differential equations," *Heat Transfer*, vol. 50, no. 4, pp. 3065–3078, 2021.

[12] A. Saeed, M. Jawad, W. Alghamdi, S. Nasir, T. Gul, and P. Kumam, "Hybrid nanofluid flow through a spinning Darcy–Forchheimer porous space with thermal radiation," *Scientific reports*, vol. 11, no. 1, pp. 1–5, 2021.

[13] M. Bilal, A. Saeed, M. M. Selim, T. Gul, I. Ali, and P. Kumam, "Comparative numerical analysis of Maxwell's time-dependent thermo-diffusive flow through a stretching cylinder," *Case Studies in Thermal Engineering*, vol. 27, p. 101301, 2021.

[14] A. Saeed, W. Alghamdi, S. Mukhtar et al., "Darcy-Forchheimer hybrid nanofluid flow over a stretching curved surface with heat and mass transfer," *PLoS One*, vol. 16, no. 5, article e0249434, 2021.

[15] P. Keblinski, J. Eastman, and D. Cahill, "Nanofluids for thermal transport," *Materials Today*, vol. 8, no. 6, pp. 36–44, 2005.

[16] J. Buongiorno, "Convective transport in Nanofluids," *Journal of Heat Transfer*, vol. 128, no. 3, pp. 240–250, 2006.

[17] N. S. Khan, P. Kumam, and P. Thounthong, "Computational approach to dynamic systems through similarity measure and homotopy analysis method for renewable energy," *Crystals*, vol. 10, no. 12, p. 1086, 2020.

[18] H. Machrafi, G. Lebon, and C. S. Iorio, "Effect of volume-fraction dependent agglomeration of nanoparticles on the thermal conductivity of nanocomposites: applications to epoxy resins, filled by SiO2, AlN and MgO nanoparticles," *Composites Science and Technology*, vol. 130, pp. 78–87, 2016.

[19] H. Machrafi and G. Lebon, "The role of several heat transfer mechanisms on the enhancement of thermal conductivity in nanofluids," *Continuum Mechanics and Thermodynamics*, vol. 28, no. 5, pp. 1461–1475, 2016.

[20] J. Sarkar, P. Ghosh, and A. Adil, "A review on hybrid nanofluids: recent research, development and applications," *Renewable and Sustainable Energy Reviews*, vol. 43, pp. 164–177, 2015.

[21] A. Ajibade, B. Jha, and A. Omame, "Entropy generation under the effect of suction/injection," *Applied Mathematical Modelling*, vol. 35, no. 9, pp. 4630–4646, 2011.

[22] A. Khan, Z. Shah, E. Alzahrani, and S. Islam, "Entropy generation and thermal analysis for rotary motion of hydromagnetic Casson nanofluid past a rotating cylinder with joule heating effect," *International Communications in Heat and Mass Transfer*, vol. 119, p. 104979, 2020.

[23] S. Islam, A. Khan, P. Kumam et al., "Radiative mixed convection flow of Maxwell nanofluid over a stretching cylinder with joule heating and heat source/sink effects," *Scientific Reports*, vol. 10, no. 1, pp. 1–18, 2020.

[24] V. Narla, K. Prasad, and J. V. Murthy, "Second-law analysis of the peristaltic flow of an incompressible viscous fluid in a curved channel," *Journal of Engineering Physics and Thermophysics*, vol. 89, no. 2, pp. 441–448, 2016.

[25] M. I. Khan, S. A. Khan, T. Hayat, S. Qayyum, and A. Alsaedi, "Entropy generation analysis in MHD flow of viscous fluid by a curved stretching surface with cubic autocatalysis chemical reaction," *The European Physical Journal Plus*, vol. 135, no. 2, p. 249, 2020.

[26] M. Sheikholeslami, T. Hayat, and A. Alsaedi, "MHD free convection of Al2O3–water nanofluid considering thermal radiation: a numerical study," *International Journal of Heat and Mass Transfer*, vol. 96, pp. 513–524, 2016.

[27] M. Sheikholeslami and M. M. Rashidi, "Non-uniform magnetic field effect on nanofluid hydrothermal treatment considering Brownian motion and thermophoresis effects," *Journal of the Brazilian Society of Mechanical Sciences and Engineering*, vol. 38, no. 4, pp. 1171–1184, 2016.

[28] M. J. Nine, B. Munkhbayar, M. S. Rahman, H. Chung, and H. Jeong, "Highly productive synthesis process of well dispersed Cu2O and cu/Cu2O nanoparticles and its thermal characterization," *Materials Chemistry and Physics*, vol. 141, no. 2-3, pp. 636–642, 2013.

[29] R. Yan, J. R. Simpson, S. Bertolazzi et al., "Thermal conductivity of monolayer molybdenum disulfide obtained from temperature-dependent Raman spectroscopy," *ACS Nano*, vol. 8, no. 1, pp. 986–993, 2014.